JOURNAL OF AIRCRAFT
Vol. 43, No. 2, March–April 2006

Aerodynamic Loads on Airfoil with Trailing-Edge Flap Pitching with Different Frequencies

Andrzej Krzysiak*
Institute of Aviation, 02-256 Warsaw, Poland
and
Janusz Narkiewicz†
Warsaw University of Technology, 00-665 Warsaw, Poland

Unsteady aerodynamic loads on NACA 0012 airfoil with a trailing-edge flap were measured in wind tunnel and calculated from a simple theoretical model. The airfoil model of 0.18 m chord length used in wind-tunnel test was oscillating in pitch about an axis located at 35% chord length from the airfoil leading edge. The length of trailing-edge flap was 22.6% of airfoil chord. The flap was also deflecting harmonically, but with frequency different from airfoil pitching motion. The influence of phase delay between airfoil angle of incidence and flap deflection at the beginning of the motion was considered. The theoretical method used for calculation of unsteady airfoil loads is based on two-dimensional, inviscid, incompressible flow model at subsonic Mach numbers. The expressions for unsteady aerodynamic loads calculations on the airfoil and on the flap were obtained in a closed form using distribution of flow velocity potential along the airfoil chord and along the flap length. Lift and aerodynamic moment measured in the wind tunnel were compared with results of calculations. The correlation between experimental and theoretical results is adequate.

Nomenclature

$a_{()n}, b_{()n}$	=	polynomials coefficients in approximation of the lift deficiency function
ab	=	distance of the airfoil aerodynamic centre from the midchord
b	=	half airfoil chord, $b = c/2$
C_D	=	drag coefficient
$C_{f/(m)}$	=	lift/(moment) deficiency function
C_L	=	lift coefficient
C_M	=	pitching-moment coefficient
c	=	airfoil chord
c_p	=	pressure coefficient
c_δ	=	position of flap hinge relative to the midchord
f	=	frequency of airfoil oscillations
f_δ	=	frequency of flap oscillations
$H(s)$	=	polynomial Nth order in the numerator of lift deficiency function approximation
$h(t)$	=	plunge translation of airfoil
$K(s)$	=	polynomial Nth order in the denominator of lift deficiency function approximation
k	=	reduced frequency, $=(\omega b)/U = (\pi f c)/U$
$L_{()}$	=	airfoil lift
M	=	Mach number
M_h	=	flap hinge moment
$M_{()}$	=	airfoil pitching moment
N	=	order of approximation of lift deficiency function
p	=	pressure
$Q(s)$	=	forcing function in flow state equation for circulatory lift
R	=	radius of helicopter rotor
Re	=	Reynolds number
r	=	distance of the blade section from the rotor axis
s	=	complex variable, $= j\omega$
$T_{()}$	=	period of oscillations
t	=	time
$U(t)$	=	freestream velocity
$W(t, x)$	=	velocity of airfoil in the x coordinate
$w(t, x)$	=	flow velocity perpendicular to the airfoil surface
$w_{()i}$	=	Fourier series coefficients of velocity distribution along the chord; $i = 0, 1, 2, 3$
x	=	distance along the chord from the leading edge
$y_{()}(s)$	=	state variable in differential equation for circulation part of the flow
$\alpha(t)$	=	airfoil angle of attack
α_0	=	mean airfoil angle of attack for harmonic motion
$\gamma_{()w}$	=	circulation in the wake
$\bar{\gamma}_{()w}$	=	complex amplitude of assumed periodic wake
Δp	=	pressure difference between upper and lower airfoil surface
Δt	=	time of angle phase lag
$\Delta\alpha$	=	amplitude of the airfoil angle of attack harmonic oscillations
$\Delta\delta$	=	amplitude of the flap angle of deflection harmonic oscillations
$\Delta\Phi$	=	difference of velocity potential Φ at the upper and the lower airfoil surfaces
$\delta(t)$	=	angle of flap deflection
δ_0	=	mean angle of flap deflection
ξ	=	coordinate along the wake
ρ	=	air density
Φ	=	flow velocity potential
ϕ	=	coefficients for flap velocity calculations
φ	=	phase shift between airfoil and flap deflections
Ω	=	helicopter rotor angular rate
$\omega_{()}$	=	angular frequency

Subscripts

d	=	flap, after correction for the length
h	=	flap hinge
0	=	total airload
α	=	airfoil

Received 18 January 2005; revision received 18 April 2005; accepted for publication 18 April 2005.

*Senior Research Scientist, Ph.D., Department of Aerodynamics, Al. Krakowska 110/114; andkrzys@ilot.edu.pl.

†Professor, D.Sc., Department of Automation and Aeronautical Systems, ITLiMS, ul. Nowowiejska 24; jnark@meil.pw.edu.pl. Associate Fellow AIAA.

δ = flap
(.) = derivative with respect to time

I. Introduction

A CONCEPT of "smart structure" in aeronautics is aimed on controlling various elements and systems of aircraft in a nonclassical, more advanced way. This concept has been extensively investigated for prospective applications to helicopter rotor and rotor blades[1] from the beginning of the 1990s. Various methods of varying shape of rotor blades are being explored, starting form controlling in "a large scale" by changing the blade camber, adding the trailing edge flap or leading edge slot,[2] to controlling in "a small scale" by varying the shape of the airfoil.[3] Similar concepts of active control of blades are also considered for application in wind-turbines design.[4]

It seems that the most substantial results in application of smart structures in helicopter rotors were achieved for the concept of actively controlled flaps mounted on the rotor blade trailing edge.[5–8] Different tasks such as performance improvement, vibration suppression, diminishing noise level, etc. are expected to be achieved by proper controlling deflection of the trailing-edge flap. Although in these research activities mainly harmonic oscillations of flap deflections are considered, it can be expected that a "smart driving mechanism" will allow obtaining controlled, arbitrary, nonharmonic motion of the trailing-edge flap, which in simulations proved to be useful for improvement of rotor performance.[9]

Aerodynamic loads play an essential role in rotor aeroelastic behavior, and so their proper modeling is an important part of research concerning the prospective application of a trailing-edge flap. Various theoretical approaches to calculate aerodynamic loads on an airfoil with trailing-edge flap were developed,[10] but it seems that there are not many experimental and theoretical results for oscillating airfoils with oscillating trailing-edge flaps published in available generally references.

The main difficulty in the evaluation of methods for unsteady loads calculation is the lack of experimental data within proper ranges of aerofoil and flap motion degrees of freedom and Mach number. It seems that up until now there were no such experimental data published in generally available publications for aerofoil and flap. It concerns especially the cases when the airfoil and the flap perform different forms of motion. This paper is aimed at contributing to fill this gap. It is composed in the following way.

First a short overview of methods available for calculations of airloads on airfoil with trailing-edge flap is presented. Then the method for the calculation of airloads on an airfoil with trailing-edge flap, both performing arbitrary motion (first time presented in Ref. 11), is briefly reviewed. This revision is necessary because of the improvements of the method, developed since its first publication.[12] In the subsequent part of the paper, the methodology and the equipment used in experimental measurements of unsteady loads on airfoil with deflecting flap are described and sample results presented. The influence of the phase shift between airfoil and flap movement at the beginning of the tests is discussed. In the final section of the paper, the comparison of experimental and theoretical results is presented. Good correlation of experimental and theoretical results is obtained, despite the simplicity of the theory. It proves the applicability of the method to unsteady load calculations in simulation of helicopter rotor-blade motion.

II. Overview of the Methods for Airfoil Unsteady Airloads Calculations

Despite the latest achievements in computational fluid dynamics (see for instance Refs. 13 and 14), the capability of solving a complete set of unsteady equations modeling the flow around an aerofoil with a trailing-edge flap both performing arbitrary, different motion is still a challenging task. A way to avoid time-consuming CFD calculations is to use simplified methods. This approach seems useful, for instance, in performing simulations of aeroelastic behavior of helicopter rotor. In the most useful methods for calculation of unsteady aerodynamic loads in aeroelastic simulations, the flow motion is described in state variables by set ordinary differential equations. It allows including such expressions directly into simulation codes for helicopter flight dynamics, rotorcraft aeroelastic analysis, as well as into codes of Floquet or eigenanalysis for stability evaluation, and for calculating gains in control algorithms. Aerodynamic models in state variables can account for arbitrary aerofoil motion and can capture history of the flow, which is inherent for unsteady aerodynamics models.

A practical method for calculating unsteady aerodynamic loads for application to helicopter rotor blade does not need to be *too* general. Up until now the assumption of a two-dimensional flow environment has been well justified. The limits of flow parameters to be covered by prospective method can be estimated taking into account average rotor data: 1) flap can be placed from $0.2R$ (due to hub elements) to $0.95R$ (due to modern advanced tips); and 2) flow velocity about in the cross section of rotor blade comes from shaft rotation and can be estimated as 220 m/s and form forward flight speed of helicopter, from which the highest value can be assumed as 300 km/h = 84 m/s, which gives a total rotor tip speed of about 300 m/s, and Mach number about 0.9.

Reduced frequency based on rotor angular velocity can be estimated as

$$k = (\omega c)/(2U) = (\Omega c)/(2\Omega r) = c/(2r) \tag{1}$$

where r is the distance of the blade cross section from the shaft axis.

So the parameters of the flow considered in modeling of unsteady airloads on helicopter rotor blade can be assumed as

$$k \in (0.04 \div 0.14), \qquad M \in (0.9 \div 0) \tag{2}$$

In the past and also now rotorcraft methods for calculating aerodynamic loads are being developed somehow parallel to fixed-wing methods, as a result of some peculiarities of rotor flow, especially vortex shape. For modeling devices mounted on the blade, the methods from fixed wing are widely adopted.

The unsteady aerofoil aerodynamic methods have been usually formulated in the frequency domain. This formulation is convenient in investigating stability for one discrete frequency. It is not appropriate in rotary-wing case, as, because of periodic excitation, there can be several frequencies at which instability can occur.

There were several overviews of methods for calculating unsteady aerofoil loads (for instance, see Ref. 15), but it is difficult to find an overview of methods specific for calculating unsteady aerodynamic loads on an aerofoil with trailing-edge flap. The statement can be found in some papers (for instance, see Ref. 16) that "extension of the method to aerofoil with flap is obvious and the work is left to the reader." So it seems worth reviewing at least some papers in which the trailing-edge flap/tab is considered.

The methods for calculating unsteady aerodynamic loads on an aerofoil with a trailing-edge flap were developed in response to the needs of current designs. The role of driving forces for the progress in development of theoretical and computational methods can be attributed (in chronological order) to augmentation of lift (steady loads), preventing flutter of aileron (flap), investigating transonic buzz, implementing systems for active flutter suppression, and now to concept of smart structure technology.

The first papers dated to the 1930s and 1940s were devoted to investigation of lift-augmenting systems, and steady airloads were considered. The overview of the static airfoil data with lists of references can be found in Refs. 17–19. In that time, the methods for unsteady loads were developed mainly in the frequency domain for investigating possibility of flutter-type instability of wings with ailerons. The classical approach for calculation of unsteady airloads on an aerofoil with a trailing-edge flap for subsonic, incompressible flow was developed by Theodorsen[20] and next extended by Theodorsen and Garrick[21] to wing aileron-flap configuration. Some papers from that period (e.g., Refs. 22 and 23) concern mainly derivatives of aerodynamic loads vs flap deflection. The important restrictions of the methods from that time in application to rotorcraft concerned assumptions of constant flow velocity, no chordwise motion, and the same motion of aerofoil and flap. The extension of

these methods made by Greenberg[16] takes into account the varying freestream velocity, but not varying flap deflection.

In the 1950s a lot of effort was spent on unsteady, transonic airloads, because of the need for preventing transonic buzz.[24,25] The experimental works[25] in NLR (The Netherlands) should be quoted here.

In the 1960s and 1970s systems for active flutter suppression evoked the need for accounting for arbitrary airfoil motion. The main papers[26,27] which appeared in that time were devoted to arbitrary flap motion relative to the fixed aerofoil. The transformation to the time domain applied for instance in Ref. 28 allows the releasing of the method limitations to harmonic motion only.

Now the main need for considering arbitrary motion of an aerofoil with a flap stems from rotorcraft activity caused by prospective application of smart structures.

In rotorcraft applications at the beginning, usually the methods used for calculations of unsteady airloads were extensions or adaptations of fixed-wing cases (see Refs. 29–31). The review of these attempts is done in Ref. 32. These extensions did not include trailing-edge flaps.

For arbitrary flap motion, the indicial function approach was developed and investigated in Refs. 33 and 34, and arbitrary motion was included as empirically justified corrections. The extension of the approach from Ref. 16 was developed in Ref. 35. In Ref. 36 previously developed state modeling using Theodorsen function was applied. A heuristic application of the ONERA stall model was applied in Ref. 9.

III. Method for Calculation of Aerodynamic Unsteady Loads

The method used in this study for comparison with experimental data was developed in 1995 in Ref. 11. Since then, the method has been improved.[12] As the improved method has not been presented in widely known journals, it is worthwhile to give description here, which would allow implementation by other authors.

The method concerns a thin, low cambered aerofoil with a flap at the trailing edge in inviscid, incompressible, two-dimensional flow (Fig. 1). Both aerofoil and flap can perform arbitrary motions, and so freestream velocity $U(t)$, airfoil plunge translation $h(t)$, aerofoil angle of incidence $\alpha(t)$, and angle of flap deflection $\delta(t)$ can be different functions of time. It is assumed that flow parameters do not exceed values at which flow separation occurs.

The potential of velocity perturbation fulfills the Laplace equation

$$\nabla^2\Phi = 0 \tag{3}$$

with the following boundary conditions: 1) on the aerofoil—a component of a flow velocity perpendicular to the aerofoil matches that of the aerofoil; 2)

$$w(x,t) = W(x,t) \tag{4}$$

3) at infinity—the perturbation of velocity potential should vanish.

The pressure difference between upper and lower airfoil surfaces is obtained from the linearized Bernoulli equation, using the velocity potential:

$$\Delta p = -\rho\left[\frac{\partial}{\partial t} + U(t)\frac{\partial}{\partial x}\right]\Delta\Phi \tag{5}$$

where $\Delta\Phi$ is the difference of velocity potential Φ at the upper and the lower airfoil surfaces $\Delta\Phi = \Phi|_U - \Phi|_L$.

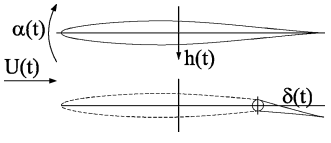

Fig. 1 Model of thin aerofoil with a trailing-edge flap performing arbitrary motion.

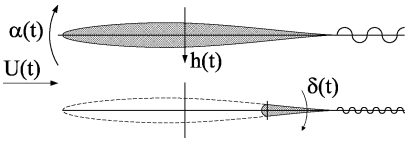

Fig. 2 Velocity decomposition for calculation of aerodynamic loads.

Lift and moment on aerofoil and flap are calculated by integrating the pressure distributions along the airfoil chord:

$$L_0(t) = \int_{-b}^{b}(-\Delta p)\,\mathrm{d}x = \rho\int_{-b}^{b}\left[\frac{\partial\Delta\Phi}{\partial t} + U(t)\frac{\partial\Delta\Phi}{\partial x}\right]\mathrm{d}x \tag{6}$$

$$M_0(t) = -\int_{-b}^{b}(-\Delta p)x\,\mathrm{d}x + abL_0(t)$$

$$= -\rho\int_{-b}^{b}\left[\frac{\partial\Delta\Phi}{\partial t} + U(t)\frac{\partial\Delta\Phi}{\partial x}\right]x\,\mathrm{d}x + abL(t) \tag{7}$$

It is assumed that lift is positive upward. Moment is positive, when the aerofoil rotates the leading edge upward. Moment is calculated relative to the midchord, assuming that aerofoil aerodynamic center is situated at a distance a from midchord.

Total unsteady loads (both lift and moment) are calculated as the sums of contributions from the aerofoil and the flap:

Total lift:

$$L_0 = L_\alpha + L_\delta \tag{8}$$

Total moment:

$$M_0 = M_\alpha + M_\delta \tag{9}$$

Flap hinge moment:

$$M_h = M_\delta(a = c_\delta) \tag{10}$$

The velocities on the airfoil (without flap motion) and on the flap itself are considered separately (Fig. 2). In this method the distribution of loads between the aerofoil and the flap is based on a velocity criterion. This is the main difference between this approach and the previous works, mainly based on spatial decomposition.

The aerodynamic loads described next as "aerofoil" result from velocities along the total aerofoil, that is, the full chord length (flap included). The flap loads stem from variation of velocity caused by the flap motion relative to the aerofoil. *As a result of this approach, the same general expressions for calculating contributions to loads from the aerofoil and from the flap are obtained.*

The airfoil bound circulation is calculated as the sum Fourier series along the chord, for which the Fourier components of airfoil velocities $w_{()}$ along the chord should be taken. For airfoil loads the velocity without flap should be taken into calculations. For calculating flap airloads, the flap velocities relative to the aerofoil should be modified according to the formulas:

$$\phi = \arccos(c_\delta/b) \tag{11}$$

$$w_{d0} = \phi w_{\delta 0} + 0.5 w_{\delta 1}\sin(\phi) \tag{12}$$

$$w_{d1} = 2w_{\delta 0}\sin(\phi) + w_{\delta 1}[\phi + 0.5\sin(2\phi)] \tag{13}$$

$$w_{d2} = w_{\delta 0}\sin(2\phi) + 0.5 w_{\delta 1}\left[\sin(\phi) + \left(\tfrac{1}{3}\right)\sin(3\phi)\right] \tag{14}$$

$$w_{d3} = \left(\tfrac{2}{3}\right)w_{\delta 0}\sin(3\phi) + 0.5 w_{\delta 1}[\sin(2\phi) + 0.5\sin(4\phi)] \tag{15}$$

Including coefficients of the Fourier series of velocity potential into Eqs. (6) and (7), the general form of expressions for aerodynamic loads are obtained for aerofoil and flap, that is,

Lift:

$$L_{()}(t) = L_{()C} + L_{()N} \tag{16}$$

$$L_{()C}(t) = 2\pi\rho Q_{()}(t) C_f(t, \gamma_{()w}) \tag{17}$$

$$L_{()N}(t) = \pi\rho b^2 \left[\dot{w}_{()0} - \left(\frac{1}{2}\right)\dot{w}_{()2} \right] \tag{18}$$

$$Q_{()}(t) = U(t)\left[w_{()0} + \left(\frac{1}{2}\right) w_{()1} \right] \tag{19}$$

$$C_{()f}[t, \gamma_{()w}] = \int_b^\infty \gamma_{()w} \left(\sqrt{\frac{\zeta + b}{\zeta - b}} - 1 \right) \mathrm{d}\zeta + \frac{1}{U(t)} \frac{\partial}{\partial t} \int_b^\infty \gamma_{()w} \left(\zeta - \sqrt{\zeta^2 - b^2} \right) \mathrm{d}\zeta \tag{20}$$

Moment:

$$M_{()}(t) = M_{()N}(t) + M_{()C}(t) \tag{21}$$

$$M_{()C}(t) = -\frac{\rho}{2} C_{()m}(t, \gamma_{()w}) + (0.5b + a) L_{()C}(t) \tag{22}$$

$$M_{()N}(t) = -\left(\frac{1}{8}\right)\pi\rho b^2 \{4U[w_{()1} + w_{()}2] + b[\dot{w}_{()1} - \dot{w}_{()3}] + 4b[\dot{w}_{()0} - 0.5\dot{w}_{()2}]\} + (0.5b + a) L_{()N}(t) \tag{23}$$

$$C_{()m}[t, \gamma_{()w}] = U(t) \int_b^\infty \gamma_{()w} \left(\varsigma - \sqrt{\varsigma^2 - b^2} \right) \left(\sqrt{\frac{\varsigma + b}{\varsigma - b}} - 1 \right) \mathrm{d}\varsigma + \frac{1}{2} \frac{\partial}{\partial t} \left[\int_b^\infty \gamma_{()w} \left(\varsigma - \sqrt{\varsigma^2 - b^2} \right)^2 \mathrm{d}\varsigma + 2b \int_b^\infty \gamma_{()w} \left(\varsigma - \sqrt{\varsigma^2 - b^2} \right) \mathrm{d}\varsigma \right] \tag{24}$$

To make use of expressions (17) and (22), the wake shape should be assumed. For a general wake shape the moment deficiency function $C_m(t, \gamma_w)$ accounting for the influence of the wake on aerofoil aerodynamic moment does not vanish.

The method presented allows calculation of loads for arbitrary motion, not only in pitch but also in heaving and lead-lad directions. These cases need assumption of the wake shape. In this paper the "Theodorsen's," that is, harmonic wake, was assumed[20] for airfoil and flab because this case was investigated experimentally.

For periodic motion of the aerofoil and the flap, the periodic time dependence of the wake shape is assumed in the form:

$$\gamma_{()w} = \bar{\gamma}_{()w} \exp\lfloor \omega_{()}(t - \zeta/U) \rfloor \tag{25}$$

It can be shown that, if there is no assumed wake distortion, the moment deficiency function $C_m[t, \gamma_{()w}]$ is half of the lift deficiency $C_f[t, \gamma_{()w}]$ function, as usually in the case of a harmonic aerofoil motion. In the frequency domain, lift deficiency function can be approximated as the fraction of polynomials:

$$C_{()f}(s) = \frac{H_{()}(s)}{K_{()}(s)} = \frac{\left(\sum_{n=0}^{N} a_{()n} s^n\right)}{\left(\sum_{n=0}^{N} b_{()n} s^n\right)} \tag{26}$$

The new state variable is assumed in the form:

$$y_{()}(s) = Q_{()}(s)/K_{()}(s) \tag{27}$$

and included into Eq. (26). Next the inverse Laplace transformation of Eq. (26) is performed, and the differential equation of Nth order for the state variable Eq. (27) is obtained in the form

$$\frac{\mathrm{d}^N y_{()}}{\mathrm{d}t^N} + \sum_{n=1}^{N-1} b_{()n} \frac{\mathrm{d}^n y_{()}}{\mathrm{d}t^n} + b_{()0} y_{()} = Q_{()}(t) \tag{28}$$

Table 1 Coefficients of approximation of lift deficiency function

n	3	2	1	0
a_n	0.50465	0.4414	0.07566	0.00189
b_n	1.0	0.6475	0.08512	0.00189

Having solved Eq. (28), the circulatory part of the lift is calculated as

$$L_{()C}(t) = 2\pi\rho b \left\{ a_{()N} U(t) \left[w_{()0} + \left(\frac{1}{2}\right) w_{()1} \right] + \sum_{n=0}^{N-1} [a_{()n} - a_N b_n] y_{()}^{(n)} \right\} \tag{29}$$

Equations (25–29) are used for airfoil and flap separately because of assumed velocity separation, so that in these expressions indices are α and δ.

It was assumed that airfoil and flap generate the same shape of the wake. It was checked by simulations that within the limits of parameters under consideration Eqs. (1) and (2) the approximation Eq. (26) of the lift deficiency function by the third-order polynomials is adequate. The coefficients of these polynomials are given in Table 1.

The comparison of the results obtained by the method described with experimental data is given in the following parts of this paper. The further method investigation and development might concern better approximation of the wake shape [Eq. (25)] and different wake shapes for the flap and the airfoil, adjusting lift-curve slope to the real values.

The method captures also the plunge motion of the airfoil, but as a result of a lack of experimental data this case is not validated.

IV. Measurement Equipment for Wind-Tunnel Tests of Airfoil with Flap

A. Experimental Equipment

In this part of the paper, the methodology for unsteady load measurement and the equipment is described. The experimental tests were performed in a trisonic N-3 wind tunnel in the Institute of Aviation (IoA) Warsaw, Poland.[37] The N-3 tunnel is a blowdown type with partial recirculation of the flow. It can operate in subsonic, transonic, and supersonic flow regimes at Mach numbers $M = 0.2$–1.2, 1.5, and 2.3. The closed test section (cross section 0.6 m × 0.6 m, length 1.58 m) can have perforated top and bottom walls for tests at subsonic and transonic flow velocities and solid walls at supersonic. Each side wall of the test section is equipped with two double windows of 0.25 m diam. During the airfoil tests, two of these windows are replaced by support of the model. The support of the model is controlled by computer, which allows changes of airfoil incidence angle within the range of 20 deg with 0.01-deg step. Static and total pressure of the undisturbed flow are measured by two independent sets of Solatron and Sonix transducers, having the range of measurement 1.3 and 2.6 bars and accuracy of 0.02% full scale. The time duration of the tests depends on wind-tunnel operating regime and is up to 15 min at subsonic speeds, up to 5 min at transonic speeds, and up to 3 min at supersonic speeds.

B. Airfoil Model

The model of NACA 0012 airfoil, used in this study, was made of steel. The dimensions of the model are shown in Fig. 3 and are given in Table 2, and in Fig. 4 the photo of the model is presented. The cavity made in the upper side of the model provides the space necessary to mount three miniature pressure scanners ESP 16HD (Pressure System). During the tests, the cavity is covered by a plate.

The ESP 16HD pressure scanner contains an array of 16 silicon piezoresistive pressure sensors, which can be multiplexed at rates up to 20.000 Hz. The accuracy of the pressure sensors is ±0.05% full scale (FS = 10 psid for two scanners and 5 psid for one scanner).

The 48 measurement orifices of 0.4 mm diam are distributed in the middle of the model span, along the chord on the upper and

Table 2 Model dimensions

Geometric quantities	Names and values
Airfoil type	NACA 0012
Airfoil chord (with flap)	0.18 m
Flap length	0.04069 m (26,15%c)
Distance of airfoil axis of rotation from airfoil leading edge	0.35c
Distance of flap hinge from the airfoil leading edge	0.8c
Radius of flap leading edge	0.00469 m
Gap between flap and airfoil (minimum)	0.0005 m
Model span (the width of wind-tunnel cross section)	0.6 m

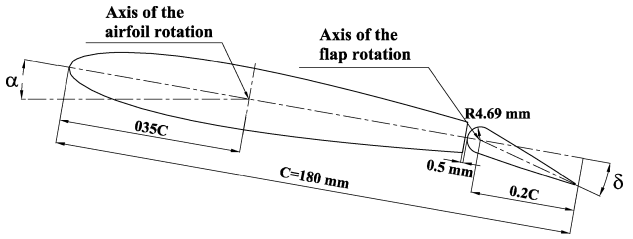

Fig. 3 Main dimensions of the airfoil model with trailing-edge flap.

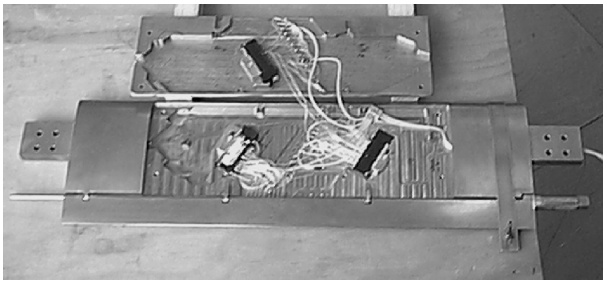

Fig. 4 Model of NACA 0012 airfoil with pressure sensors scanners.

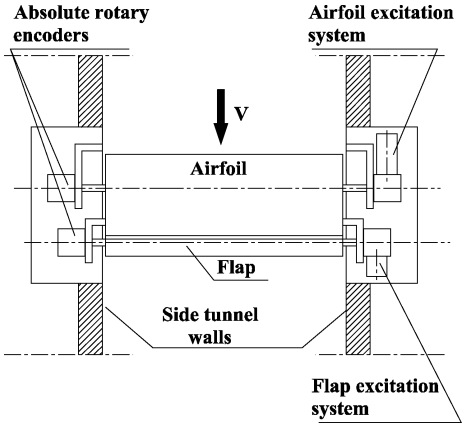

Fig. 5 Mounting of the model in wind-tunnel test section.

lower surfaces of the airfoil and the flap. The orifices are connected to the pressure scanners by the elastic pipes all of the same length 100 mm.

C. Driving System

The flap is mounted to the main part of the model by four hinges. The flap is driven by a shaft placed on the hinge axis. The hinges allow flap rotation in the range of ±90 deg, but within this study the flap deflection was ±15 deg. In Fig. 5 the mounting of the model in the wind tunnel is shown, and in Fig. 6 the model during tests of simulated icing conditions is presented.

Driving system (Fig. 7) excites independently oscillations of the airfoil and the flap. It consists of the two crank-shaft assemblies, driven by dc motors (with the range of rotations from 0 up to 6000 rpm) connected by reduction gears (1:10). During the tests, the driving system replaces the side covers (windows) of the test section.

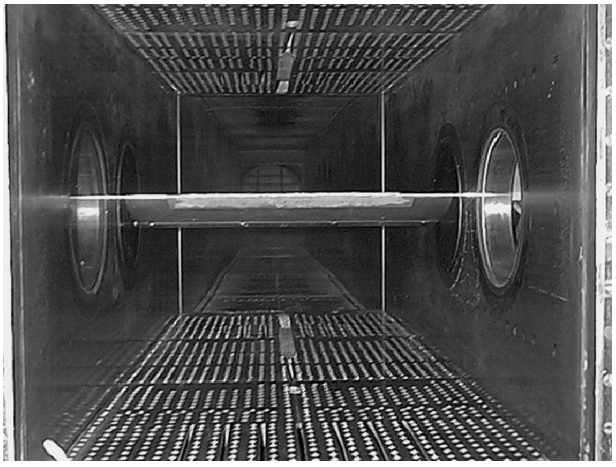

Fig. 6 Model of the airfoil in N-3 wind tunnel.

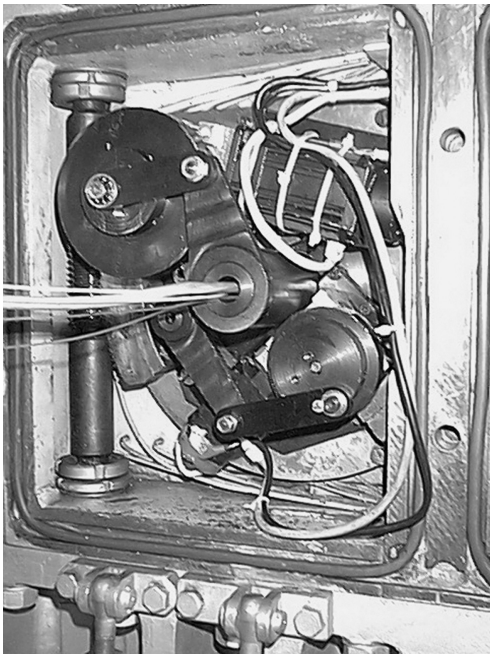

Fig. 7 Driving system of airfoil and flap.

The frequencies of oscillations of the airfoil and of the flap are changed by changing the motor rpm. The driving system allows the obtaining of the frequency of the airfoil oscillations in continuous way from 0 to 10 Hz (so, for $M = 0.4$ the reduced frequency k can vary from $k = 0$ to 0.042) and frequency of the flap oscillation from 0 to 12 Hz. The amplitudes of the airfoil and flap oscillations might be changed by changing the place on the flywheels, where the cranks are fixed. Instantaneous values of the airfoil angle of attack and the angle of the flap deflection are measured by two rotation sensors ROC 412 (Heidenhain) with max instrumental error ±0.1 deg.

D. Data-Acquisition Procedure

The data acquisition and processing was done in the subsequent steps. The system collected and registered values of pressure at 48 points distributed on the model surface along its chord during 10 periods of airfoil oscillations for each model and flow settings (M, α_0, δ_0, $\Delta\alpha$, $\Delta\delta$, f, f_f). During one period, about 25 measurements at each of the 48 points, in regular time intervals, were done. By interpolating these values, the variation of pressure in time at each measurement point was obtained. Basing on the results obtained during 10 periods of airfoil oscillations, the average pressure variations in time at each measurement point were determined. The lift C_L and moment C_M coefficients in any time were calculated by integrating pressure distributions along the chord.

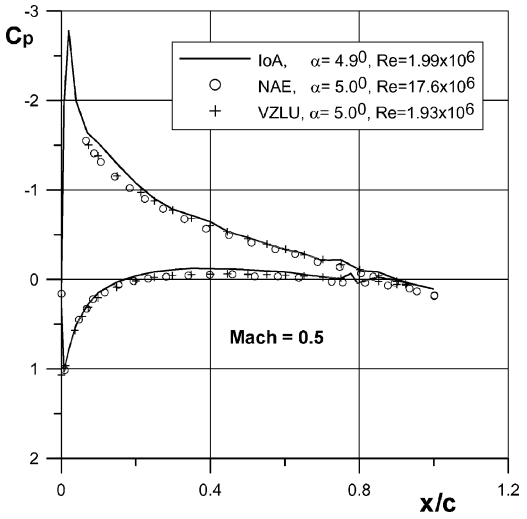

Fig. 8 Comparison of static-pressure distributions on NACA 0012 airfoil measured in various wind tunnels.

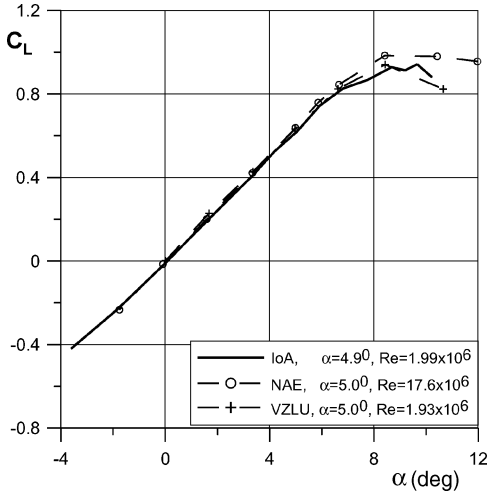

Fig. 9 Comparison of NACA 0012 airfoil of static lift coefficient vs angle of attack measured in various wind tunnels.

V. Unsteady Wind-Tunnel Tests of Airfoil with Flap

A. Comparison of Static and Dynamic Test Results

To confirm the quality and reliability of experimental tests in the Institute of Aviation wind tunnel, the comparison was done of static and dynamic results of NACA 012 airfoil tests with results obtained in other wind tunnels. In Fig. 8 the comparison is shown of static chordwise pressure distributions obtained in IoA,[37] Aeronautical Research and Tests Institute, Czech Republic,[38] National Aeronautical Establishment, Canada[39] for $M = 0.5$ and $\alpha = 5$ deg. The static lift coefficients vs angle of attack measured in the same institutions are shown in Fig. 9.

In Fig. 10 the comparison of NACA 0012 lift coefficient vs angle of attack for dynamic conditions measured in IoA and U.S. Army Air Mobility R&D Laboratory, Moffett Field, California (U.S.AAM&D L)[39] wind tunnel is presented. The airfoil performed the harmonic pitching motion, Eq. (30):

$$\alpha(t) = \alpha_0 + \Delta\alpha \sin(\omega t) \tag{30}$$

with $\alpha_0 = 15$ deg and $\Delta\alpha = 10$ deg.

This comparison is a qualitative type as a result of the differences in test conditions. But it is clear that the testing methodology applied in the Institute of Aviation captures the main features of unsteady phenomena.

Despite the differences in test conditions (Reynolds number, angle of attack) the correlation of the results obtained in Institute of Aviation with the results from other wind tunnels is good, which justifies the reliability of the data obtained for the unsteady case.

Table 3 Test conditions for unsteady airloads measurements

Parameter	Value	Measurement errors
Mach number M	0.4, 0.6	0.005
Reynolds number Re	1.63 10^6 ($M = 0.4$) 2.35 10^6 ($M = 0.6$)	——
Mean airfoil angle of attack α_0, deg	−4–15	0.15
Mean angle of flap deflection δ_0, deg	0	0.15
Nominal amplitude of the airfoil oscillations $\Delta\alpha$, deg[a]	±5	0.25
Nominal amplitude of the flap oscillations $\Delta\delta$, deg[a]	±5, ±10, ±15	0.25
Frequency of the airfoil oscillations f, Hz	5	0.1
Reduced frequency k	0.021 ($M = 0.4$) 0,014 ($M = 0.6$)	——
Frequency of the flap oscillations f_δ, Hz	10	0.1

[a]Because of torsional deflections of the model mounting during oscillations, the real amplitudes of the airfoil and flap oscillations were a little greater than nominal and equal $\Delta\alpha \approx \pm 6$ deg, $\Delta\delta \approx \pm 5.4$ deg, ± 11.3 deg, and ± 18.4 deg.

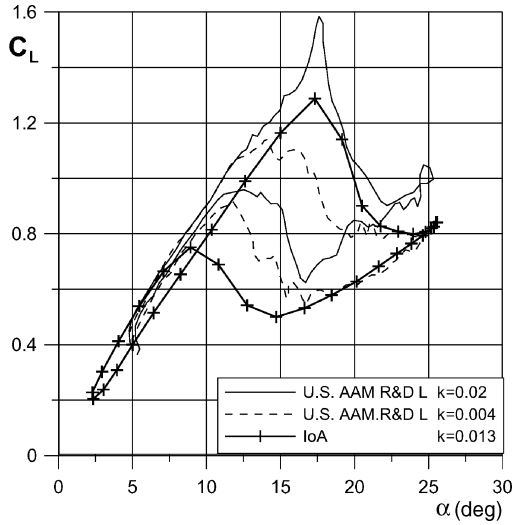

Fig. 10 Comparison of lift coefficient vs angle of attack for dynamic conditions. NACA 0012 airfoil oscillating in pitch $\alpha = 15$ deg + 10 deg $\sin(\omega t)$.

B. Conditions of the Unsteady Tests of Airfoil with Flap

In Table 3 the test conditions are given for the experimental investigation of unsteady aerodynamic loads on the pitching airfoil NACA 0012 with oscillating flap.

C. Sample Test Results

The main objective of the wind-tunnel tests was to develop measurement methodology and obtain the first set of data for comparison with the various computational methods. But the analysis of the data show some new features of the aerodynamic loads not investigated before.

The aerodynamic coefficients obtained during wind-tunnel tests results are sensitive to the phase shift between airfoil and flap oscillations. Because of different frequencies of airfoil and flap oscillations, the phase shift, related to the period of the flap oscillation T_δ between airfoil and flap motion, was defined (in degrees) as

$$\varphi = 360 \text{ deg}(\Delta t / T_\delta) = 360 \text{ deg} \Delta t f_\delta \tag{31}$$

where Δt is a time of phase lag between airfoil and flap oscillations shown in Fig. 11 (for $\alpha_0 = 0$ deg and $\delta_0 = 0$ deg).

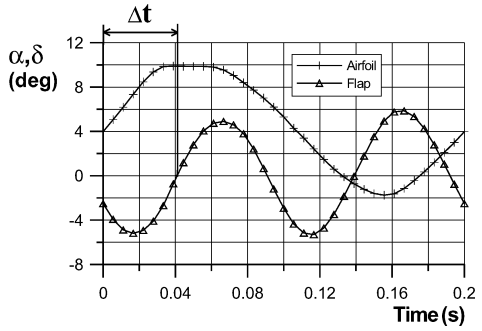

Fig. 11 Definition of the phase shift between airfoil and flap oscillations.

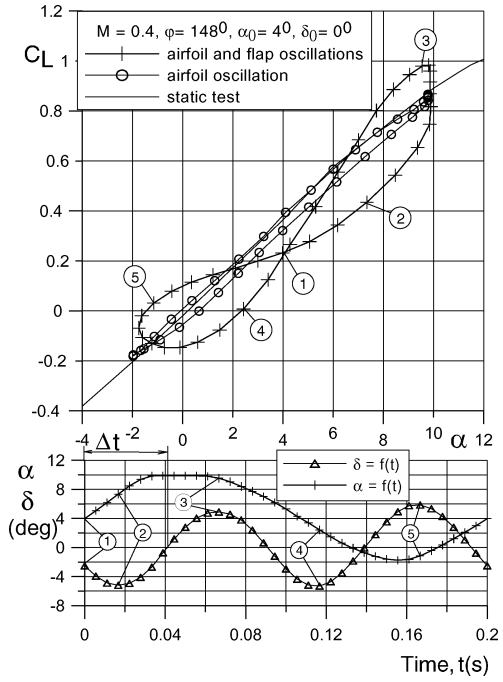

Fig. 12 Lift vs angle of attack at $\varphi = 148$ deg and $\alpha_0 = 4$ deg.

To estimate the influence of the phase shift on C_L and C_M, 20 repetitions of measurements were performed for the airfoil oscillations with the mean angle $\alpha_0 = 4$ deg, amplitude $\Delta\alpha = 6$ deg, flap mean amplitude $\delta_0 = 0$ deg, amplitude $\Delta\delta = 5.4$ deg, and various phase shift angles. In Figs. 12–14 the lift coefficients as functions of angle of attack, for static case, oscillating airfoil only, and simultaneously oscillating airfoil and flap with phase shifts $\varphi = 148$, 298, and 357 deg are shown. Below these, the variation of the angle of attack α and flap deflection δ vs time t during the one period of the airfoil oscillation are shown. The points corresponding to the extreme values of $\delta = f(t)$ are marked by successive numbers: ①, ②, . . . , ⑤. The same points are marked on the plot of lift coefficients. It is clear that lift coefficient functions of angle of attack obtained for simultaneously oscillating airfoil and flap have the shape of dual loop. The shapes of these loops depend on the angle of the phase shift. It may also be noticed that the width of lift coefficient loops is smallest (for instance, see Fig. 13) when extreme values of $\alpha = f(t)$ coincide with the extreme values $\delta = f(t)$, that is, when the maximum or the minimum of the airfoil angle of attack occurs in the same time moment as the maximum or minimum of the flap deflection. It takes place for the phase shift angles $\varphi \approx 90$ and 270 deg.

The phase shift between airfoil and flap oscillations significantly influences the maximum value of lift coefficient. When the airfoil angle of attack and angle of flap deflection increase simultaneously, the maximum lift coefficient is greater than for the pitching airfoil and nondeflecting flap. This dynamic case occurs for the phase shift $\varphi \approx 0$–50 deg and $\varphi \approx 270$–360 deg (Fig. 15). For these values of the phase shift, the highest lift coefficient value is about 1.25, comparing

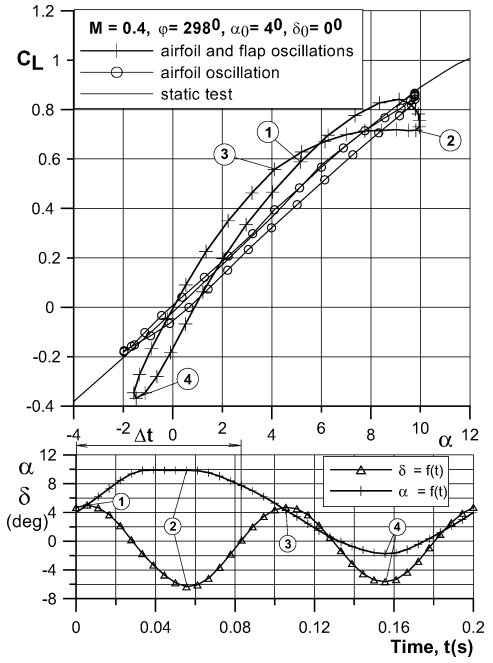

Fig. 13 Lift vs angle of attack at $\varphi = 298$ deg and $\alpha_0 = 4$ deg.

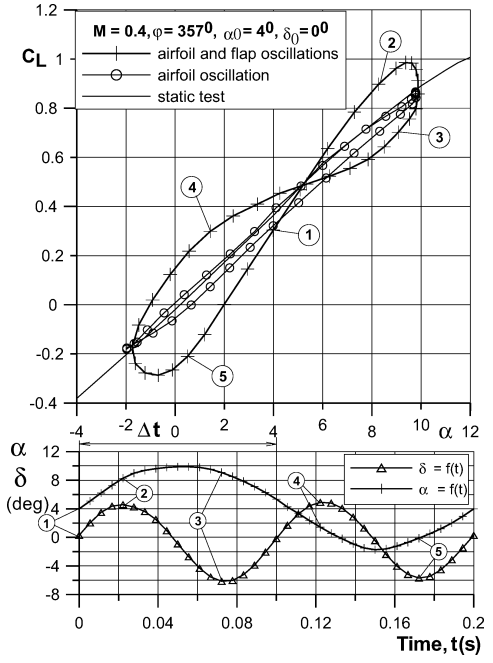

Fig. 14 Lift vs angle of attack at $\varphi = 357$ deg and $\alpha_0 = 4$ deg.

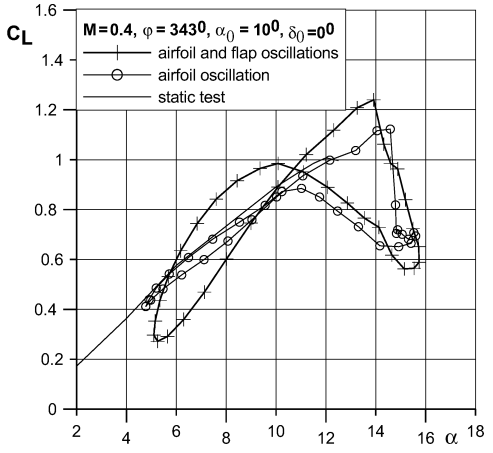

Fig. 15 Lift vs angle of attack at $\varphi = 343$ deg and $\alpha_0 = 10$ deg.

to the value 1.13 when the flap is not deflecting. For the phase-shift values in the range $\varphi \approx 100$–220 deg when the airfoil angle of attack and the angle of flap deflection simultaneously decrease, the maximum lift coefficient (Fig. 16) diminishes to 1.05.

From analysis of other results (not shown here), it can be concluded that when for given values of phase shift the maximum lift coefficient increases the value of critical airfoil angle of attack slightly diminishes (for about 0.5 deg). When for given shift values the maximum lift coefficient diminishes, the value of critical airfoil angle of attack increases a little (for about 0.2 deg).

Pitching-moment coefficient vs angle of attack α, obtained in condition of oscillating airfoil and flap, has also the form of dual loops. The shape of these loops and their intersection point change (Figs. 17 and 18), depending on the value of the phase shift angle φ.

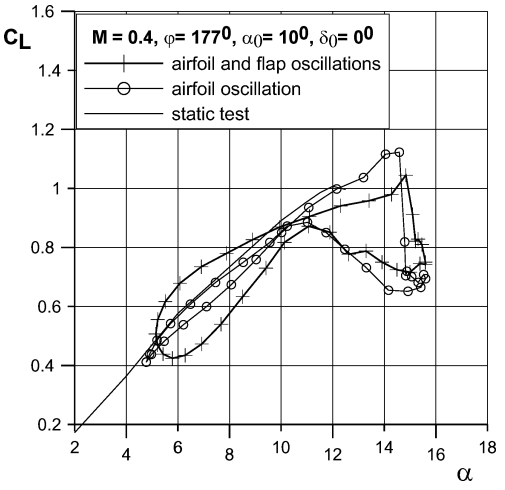

Fig. 16 Lift vs angle of attack at $\varphi = 177$ deg and $\alpha_0 = 10$ deg.

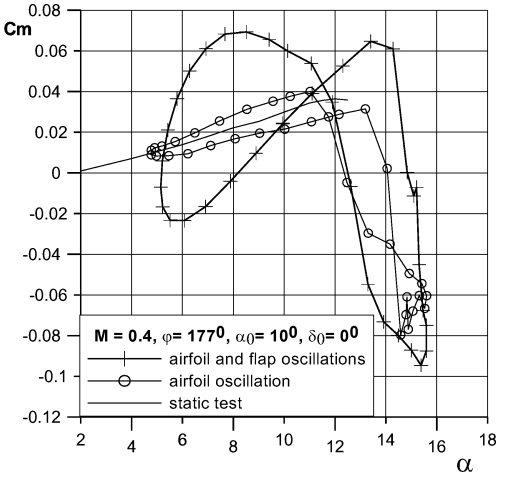

Fig. 17 Pitching moment vs angle of attack at $\varphi = 177$ deg and $\alpha_0 = 10$ deg.

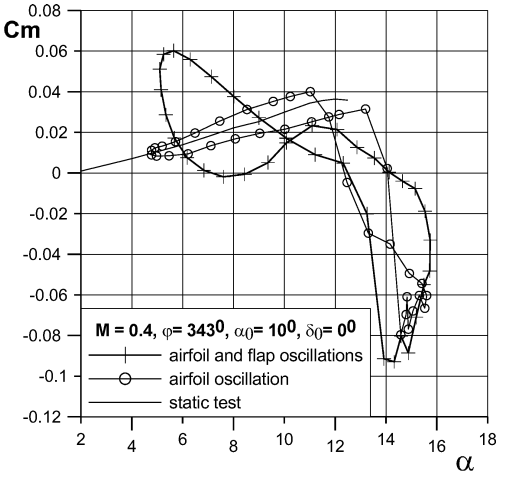

Fig. 18 Pitching moment vs angle of attack at $\varphi = 343$ deg and $\alpha_0 = 10$ deg.

VI. Comparison of Test Results with the Theory

A. Reconstruction of Airfoil and Flap Motion

In calculations of airloads, the parameters of airfoil and the flap motion are needed as input values. During the tests, the airfoil angles of attack and the flap deflections were stored in the memory in 37 discrete time moments. But there was no registration of rates and angular accelerations needed by the theory. The harmonic formulas for airfoil and flap motion were assumed in the form:

$$\alpha = \alpha_0 + \Delta\alpha \sin(\omega_\alpha t + \varphi_\alpha), \qquad \delta = \delta_0 + \Delta\delta \sin(\omega_\delta t + \varphi_\delta) \quad (32)$$

The frequencies of the airfoil and the flap motion were known. The "real" motion of the model was reconstructed in two ways.

In the first method the functions $\alpha(t)$ and $\delta(t)$ were plotted for the "nominal" values of parameters. Then by trials and errors the values of phase shift and amplitude were adjusted for the best fitting of the experimental and calculated points.

In the second method the values of angles of attack and flap deflections from experimental data were used for calculating the rates and the angular accelerations by numerical differentiating with respect to time.

B. Theory vs Experiment

In Figs. 19–27 comparisons of the results of calculation with the wind-tunnel tests are presented for various phase-shift angles

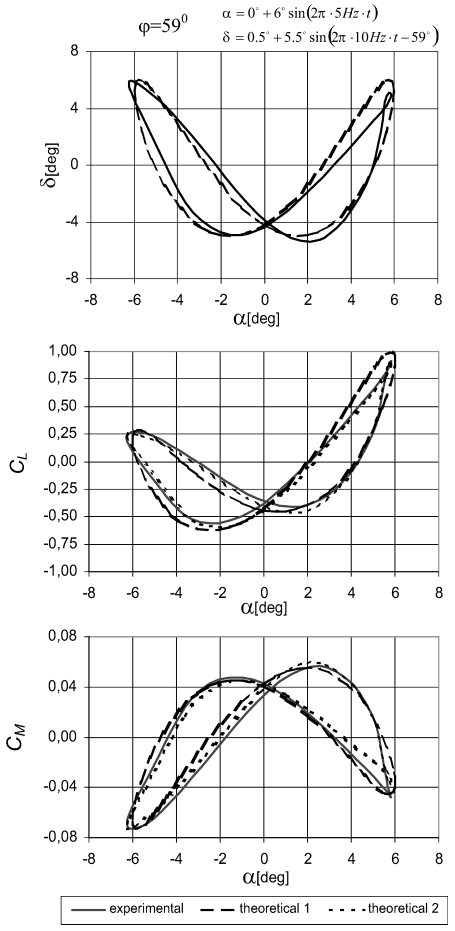

Fig. 19 Comparison of calculations with the wind-tunnel tests at small airfoil angles and $\varphi = 59$ deg.

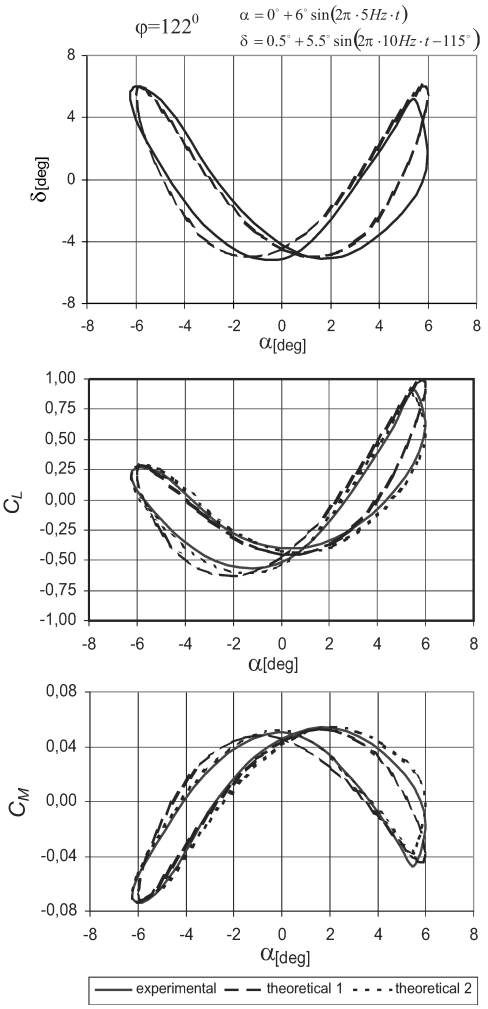

Fig. 20 Comparison of calculations with the wind-tunnel tests at small airfoil angles and $\varphi = 122$ deg.

between flap and airfoil motions and the methods of reconstruction of airfoil motion. In each group of plots, the data (solid line) and the results of calculations using the first (dashed lines) and the second (dotted lines) method of reconstruction of airfoil/flap motion are shown. For a clearer view of the differences, the experimental points are not given in comparison with calculations.

Within the first group of plots (Figs. 19–21), the airfoil and flap performed a small angle motion $\alpha_0 = 0$ deg, $\Delta\alpha = 6$ deg, $\delta_0 = 0.5$ deg, $\Delta\delta = 5.5$ deg well within the assumptions of the theory. The correlation of theoretical results with experimental data is excellent. The theory captures the loop shapes changes with the variations of phase shift. The importance of proper accounting for airfoil/tab motion is also visible.

The second group of plots (Figs. 22–24), which concerns the moderate angles $\alpha_0 = 5$ deg, $\Delta\alpha = 5.5$ deg, $\delta_0 = 0.5$ deg, $\Delta\delta = 5$ deg, shows good qualitative agreement with experimental data and good moment correlation.

The third group (Figs. 25–27) concerns the range of high airfoil angles of attack, $\alpha_0 = 11$ deg, $\Delta\alpha = 5.5$ deg, $\delta_0 = 0.5$ deg, $\Delta\delta = 4.75$ deg, within the dynamic-stall region. The method captures the changes of loads with the variation of airfoil/flap motion, but the correlation is not adequate. It is somehow a predictable effect because this case lays outside the assumptions of the theory.

Within this research there were no special attempts to adjust the model used in calculation to experimental data. There is still a possibility of improving correlation of the theoretical method with the test results using better description of the airfoil wake, taking into account the influence of Mach number and using the real static airfoil data.

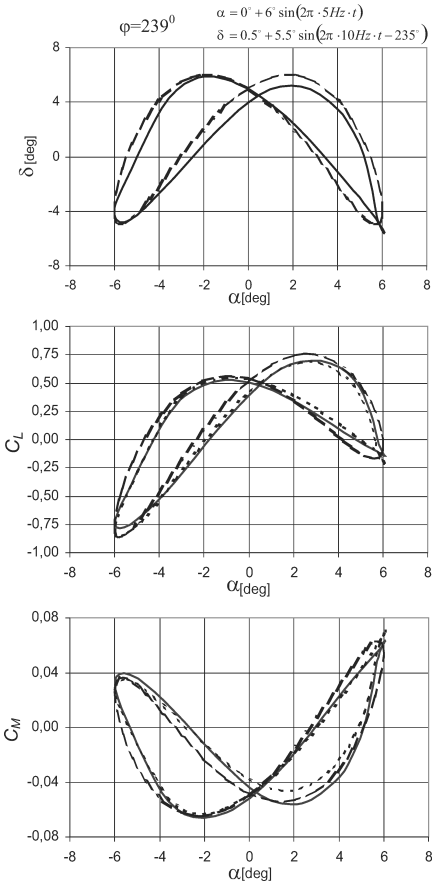

Fig. 21 Comparison of calculations with the wind-tunnel tests at small airfoil angles and $\varphi = 239$ deg.

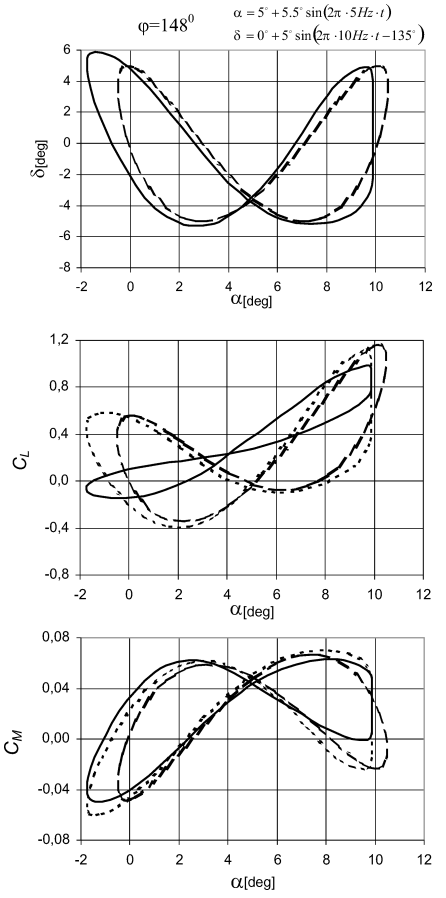

Fig. 22 Comparison of calculations with the wind-tunnel tests at moderate airfoil angles and $\varphi = 148$ deg.

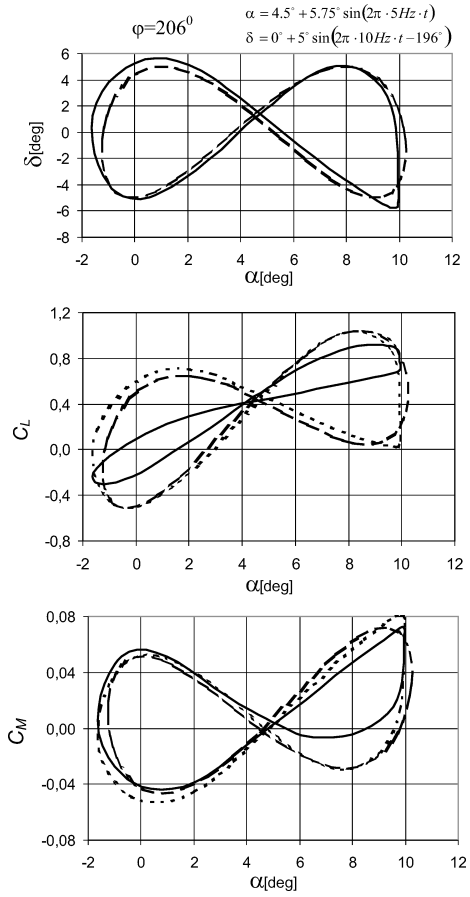

Fig. 23 Comparison of calculations with the wind-tunnel tests at moderate airfoil angles and $\varphi = 206$ deg.

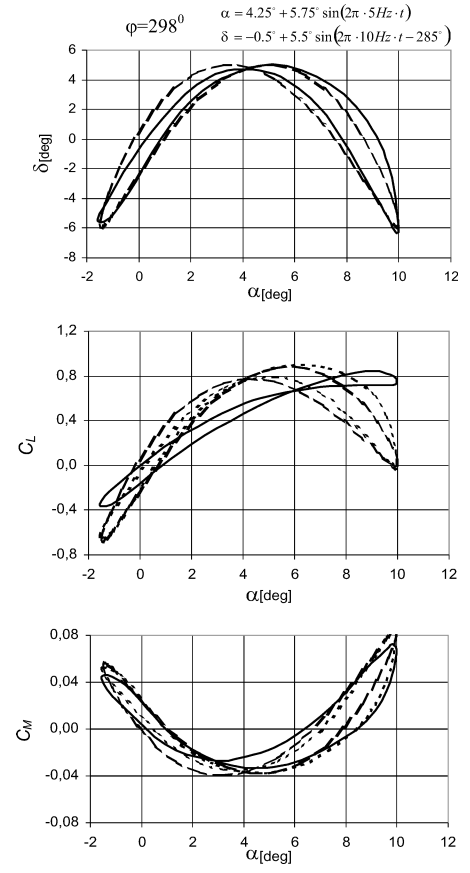

Fig. 24 Comparison of calculations with the wind-tunnel tests at moderate airfoil angles and $\varphi = 298$ deg.

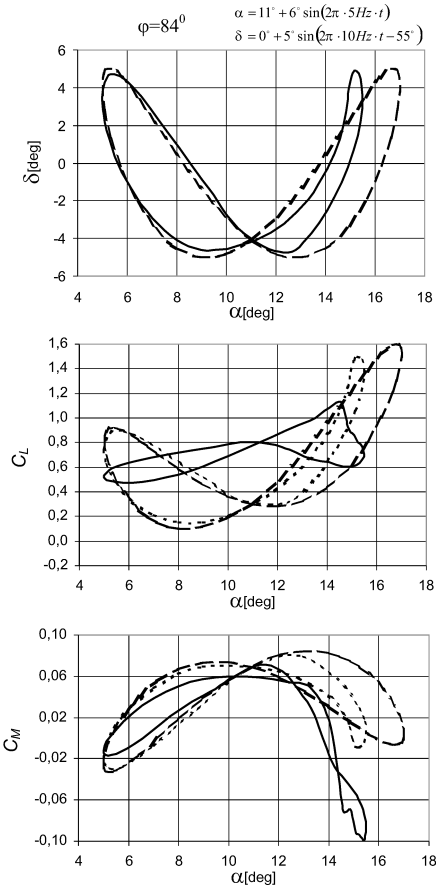

Fig. 25 Comparison of calculations with the wind-tunnel tests at high airfoil angles and $\varphi = 84$ deg.

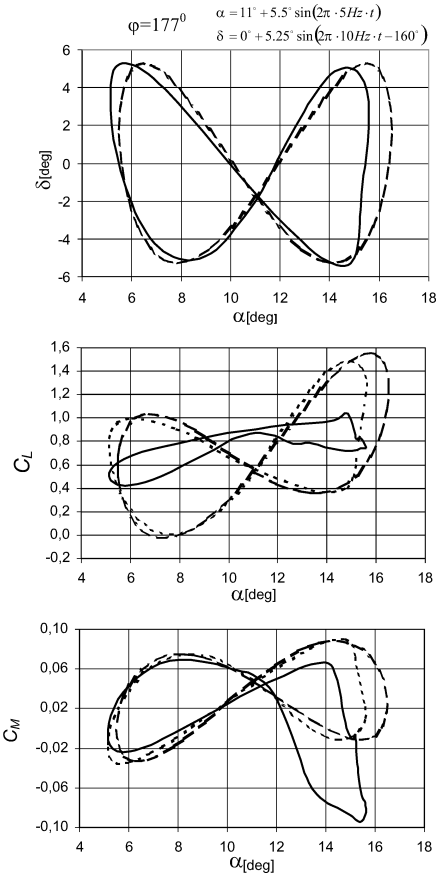

Fig. 26 Comparison of calculations with the wind-tunnel tests at high airfoil angles and $\varphi = 177$ deg.

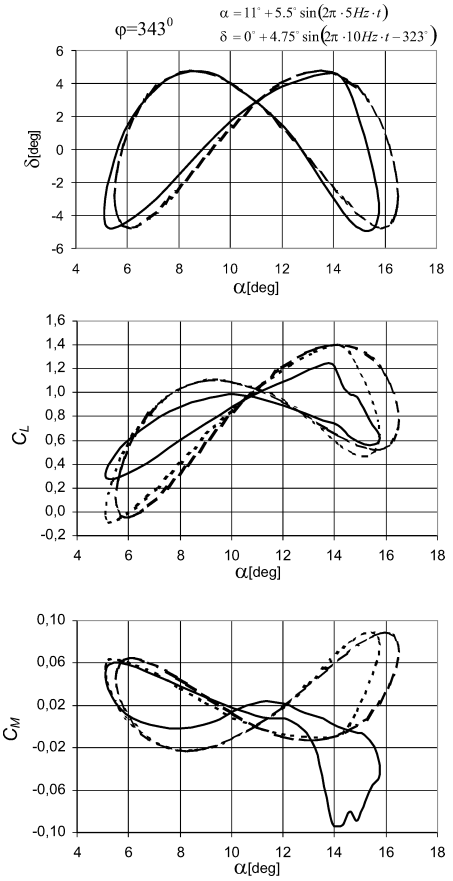

Fig. 27 Comparison of calculations with the wind-tunnel tests at high airfoil angles and $\varphi = 343$ deg.

VII. Conclusions

The results of the experimental measurements and calculations of aerodynamic loads on the pitching NACA 0012 airfoil with deflecting trailing edge flap are presented. The airfoil and the flap perform harmonic motion but with different frequencies. The phase shift of airfoil and flap at the beginning of the motion is also implemented.

The plots of lift and moment vs angle of attack obtained in the test conditions have a form of dual loops. The shapes of these loops depend on the phase-shift angle between airfoil and flap motion. The tests revealed significant influence of the phase shift between airfoil and flap oscillations on the lift and pitching-moment coefficients.

Flap oscillations (with pitching airfoil) cause an increase of maximum lift coefficient, when the angle of attack of the airfoil and flap deflection increase simultaneously; for values of phase-shift angles $\varphi \approx 0$–50 deg and $\varphi \approx 270$–360 deg, the increase of lift coefficient was about 0.12 compared to unsteady airfoil with no flap deflection. When the airfoil angle of attack and angle of flap deflection decrease simultaneously, the maximum lift coefficient diminishes for about 0.08 for the phase-shift angles $\varphi \approx 100$–220 deg.

The wind-tunnel results were compared with numerical calculation using the simple theoretical method of calculating unsteady aerodynamic loads on airfoil with deflecting flap for arbitrary airfoil and flap deflections. The correlation is adequate.

Acknowledgments

The experimental tests were done under a grant from Polish State Committee of Scientific Research "Experimental and Numerical Investigation of Dynamic Stall on Helicopter Airfoils with Influence of Icing Effect," Grant 9T12C03017.

References

[1]Chopra, I., "Status of Application of Smart Structures Technology to Rotorcraft Systems," *Journal of the American Helicopter Society*, Vol. 45, No. 4, 2000, pp. 228–252.

[2]Friedmann, P. P., "Rotary-Wing Aeroelasticity: Current Status and Future Trends," *AIAA Journal*, Vol. 42, No. 10, 2004, pp. 1953–1972.

[3]Geissler, W., Sobieczky, H., and Trenker, M., "New Rotor Airfoil Design Procedure for Unsteady Flow Control," *Proceedings of the 26th European Rotorcraft Forum*, Paper No. 31, 2000, pp. 31.1–31.9.

[4]Mannur, J., Sundaresan, M. J., Mark, J., Schulz, M. J., Ghosha, A., Laxson, A., Musial, W., Hughes, S., and Almeida, T., "An Intelligent Blade for Wind Turbines," AIAA Paper 2001-0026, 2001.

[5]Zhang, J., Smith, E. C., and Wang, K. W., "Active-Passive Hybrid Optimisation of Rotor Blades with Trailing Edge Flaps," *Journal of the American Helicopter Society*, Vol. 49, No. 1, 2004, pp. 54–65.

[6]Shen, J., and Chopra, I., "A Parametric Design Study for a Swashplateless Helicopter Rotor with Trailing Edge Flaps," *Journal of the American Helicopter Society*, Vol. 49, No. 1, 2004, pp. 43–53.

[7]Celi, R., "Stabilisation of Helicopter Blades with Severed Pitch Links Using Trailing Edge Flaps," *Journal of Guidance, Control, and Dynamics*, Vol. 26, No. 4, 2003, pp. 585–592.

[8]Shen, J., and Copra, I., "Swashplateless Helicopter Rotor with Trailing Edge Flaps," *Journal of Aircraft*, Vol. 41, No. 2, 2004, pp. 208–214.

[9]Narkiewicz, J., and Rogusz, M., "Smart Flap for Helicopter Rotor Blade Performance Improvement," *Proceedings of the 19th European Rotorcraft Forum*, Paper G9, 1993, pp. G9.1–G9.11.

[10]Leishman, G. J., *Principles in Helicopter Aerodynamics*, Cambridge Aerospace Series, Cambridge Univ. Press, Cambridge, U.K., 2000, Chap. 8.

[11]Narkiewicz, J., Ling, A., and Done, G. T. S., "Unsteady Aerodynamic Loads on an Aerofoil with a Deflecting Tab," *The Aeronautical Journal*, Vol. 99, No. 987, 1995, pp. 282–292.

[12]Narkiewicz, J., "Modeling of Unsteady Aerodynamic Loads on Aerofoil with a Trailing Edge Tab," *Research Bulletin of the Institute of Aeronautics and Applied Mechanics*, Warsaw Univ. of Technology, Poland, No. 6, 1997, pp. 253–258.

[13]Geissler, W., Dietz, G., and Mai, H., "Dynamic Stall on Supercritical Airfoil," *Proceedings of the 29th European Rotorcraft Forum*, Paper 51, 2003, pp. 51.1–51.11.

[14]Trenker, M., "Design Concepts for Adaptive Airfoils with Dynamic Transonic Flow Control," *Journal of Aircraft*, Vol. 40, No. 4, 2003, pp. 734–740.

[15]McCroskey, W. J., "Unsteady Airfoils," *Annual Review of Fluid Mechanics*, Vol. 14, 1982, pp. 285–311.

[16]Greenberg, J. M., "Airfoil in Sinusoidal Motion in a Pulsating Stream," NACA TN 1326, June 1947.

[17]Calhill, J. F., "Summary of Section Data on Trailing Edge High-Lift Devices," NACA Rept. 938, 1949.

[18]Bryant, L. W., Halliday, A. S., and Batson, A. S., "Two-Dimensional Control Characteristics," Aeronautical Research Council, ARC R&M 2730, London, March 1950.

[19]Abbot, I. H., and von Doenhoff, A. E., *Theory of Wing Sections*, Dover, New York, 1959.

[20]Theodorsen, T., "General Theory of Aerodynamic Instability and the Mechanism of Flutter," NACA Rept. 496, 1935.

[21]Theodorsen, T., and Garrick, I. E., "Nonstationary Flow About a Wing-Aileron-Flap Combination Including Arodynamic Balance," NACA Rept. 736, 1942.

[22]Turner, M. J., and Rabinowitz, S., "Aerodynamic Coefficients for an Oscillating Airfoil with Hinged Flap with Tables for a Mach Number of 0.7," NACA TN 2213, Oct. 1950.

[23]Sinnot, C. S., "Hinge-Moment Derivatives for an Oscillating Control," Aeronautical Research Council, ARC R&M 2923, London, 1953.

[24]Hassig, H. J., "Aerodynamic Flutter Coefficients for an Airfoil with Leading- and Trailing-Edge Flaps in Two-Dimensional Supersonic Flow," *Journal of the Aeronautical Sciences*, Vol. 12, No. 2, 1954, pp. 131, 132.

[25]Tijdeman, H., "Investigation of the Transonic Flow Around Oscillating Airfoils," National Aerospace Lab., NLR TR 77090 U, Amsterdam, Oct. 1977.

[26]Rowe, W. S., Winther, B. A., and Redman, M. C., "Unsteady Subsonic Aerodynamic Loading Caused by Control Surface Motion," *Journal of Aircraft*, Vol. 11, No. 1, 1974, pp. 45–54.

[27]Edwards, J. W., "Unsteady Aerodynamic Modelling and Active Aeroelastic Control," NASA CR-148019, Feb. 1977.

[28]Edwards, J. W., Ashley, H., and Breakwell, J. V., "Unsteady Aerodynamic Modelling for Arbitrary Motions," *AIAA Journal*, Vol. 17, No. 4, 1979, pp. 365–374.

[29]Johnson, W., "Application of Unsteady Airfoil Theory to Rotary Wings," *Journal of Aircraft*, Vol. 17, No. 4, 1980, pp. 285, 286.

[30]Kottapalli, S. B. R., "Unsteady Aerodynamics of Oscillating Airfoils with In plane Motion," *Journal of the American Helicopter Society*, Vol. 30, No. 1, 1985, pp. 62, 63.

[31]Kaza, K. R. V., and Kvaternik, R. G., "Application of Unsteady Airfoil Theory to Rotary Wings," *Journal of Aircraft*, Vol. 18, No. 7, 1981, pp. 604, 605.

[32]Bielawa, R., *Rotary Wing Structural Dynamics and Aeroelsticity*, AIAA Education Series, AIAA, Washington, DC, 1995, Chap. 12.

[33]Harriharan, N., and Leishman, G. J., "Unsteady Aerodynamics of a Flapped Airfoil in Subsonic Flow by Indicial Concept," *Journal of Aircraft*, Vol 33, No. 5, 1996, pp. 855–868.

[34]Leishman, J. G., "Unsteady Lift of an Airfoil with a Trailing-Edge Flap Based on Indicial Concepts," *Proceedings of the 18th European Rotorcraft Forum*, Paper 19, Sept. 1992, pp. 19.1–19.14.

[35]Myrtle, T. F., and Friedmann, P. P., "Application of a New Compressible in Time Domain Aerodynamic Model to Vibration Reduction in Helicopters Using an Actively Controlled Flap," *Journal of the American Helicopter Society*, Vol. 46, No. 1, 2001, pp. 32–43.

[36]Peters, D. A., and Johnson, M. J., "Finite State Airloads for Deformable Airfoils on Fixed and Rotating Wings," *Proceedings of the ASME Winter Annual Meeting*, AD-Vol. 44, 1994, pp. 1–28.

[37]Krzysiak, A., "Experimental and Numerical Investigation of Dynamic Stall on Helicopter Airfoils with Influence of Icing Effect," Warsaw Inst. of Aviation, Internal Rept., 51/BA/01/P, Dec. 2001 (in Polish).

[38]Benetka, J., Kladrubsky, M., and Valenta, R., "Mereni Profilu NACA 0012 ve Stebinovem Mericim Prostoru," Internal Rept. VZLU R-2909/98 Praha, Czech Republic, April 1998.

[39]Carr, L. W., McAlister, K. W., and McCroskey, W. J., "Analysis of Development of Dynamic Stall Based on Oscillating Airfoil Experiments," NASA TN D-8382, Jan. 1977.